Naturally Occurring Nanoparticles from *Arthrobotrys oligospora* as a Potential Immunostimulatory and Antitumor Agent

*Yongzhong Wang, Leming Sun, Sijia Yi, Yujian Huang, Scott C. Lenaghan, and Mingjun Zhang**

***Arthrobotrys oligospora*, a representative flesh eater in the fungal kingdom, is a potential source for natural-based biomaterials due to the presence of specialized 3D adhesive traps that can capture, penetrate, and digest free-living nematodes in diverse environments. The purpose of this study is to discover novel nanoparticles that occur naturally in *A. oligospora* and to exploit its potential biomedical applications. A new culture method, fungal sitting drop culture method, is established in order to monitor the growth of *A. oligospora* in situ, and observe the nanoparticle production without interfering or contamination from the solid media. Abundant spherical nanoparticles secreted from the fungus are first revealed by scanning electron microscopy and atomic force microscopy. They have an average size of 360–370 nm, with a zeta potential of –33 mV at pH 6.0. Further analyses reveal that there is ≈28 μg of glycosaminoglycan and ≈550 μg of protein per mg of nanoparticles. Interestingly, the nanoparticles significantly induce TNF-α secretion in RAW264.7mouse macrophages, indicating a potential immunostimulatory effect. The nanoparticles themselves are also found slightly cytotoxic to mouse melanoma B16BL6 and human lung cancer A549 cells, and show a synergistic cytotoxic effect upon conjugation with doxorubicin against both cells. This study proposes a new approach for producing novel organic nanoparticles secreted from microorganisms under controlled conditions. The findings here also highlight the potential roles of the naturally occurring nanoparticles from *A. oligospora* as an immunostimulatory and antitumor agent for cancer immunochemotherapy.**

1. Introduction

Naturally occurring inorganic nanoparticles, from a variety of sources, have been extensively studied.[1] These nanoparticles have been found in soil, ground and surface waters, volcanic ash, ocean spray, mineral composites, smoke, etc.[2] Biogenic magnetite nanoparticles have even been discovered in various organisms, ranging from bacteria to human brains, with various biological functions.[3] However, naturally occurring organic nanoparticles have only recently drawn significant interest from scientific communities, due to their unique properties and increased biocompatibility. In 2008, our group first discovered that ivy secreted organic nanoparticles, and that these nanoparticles aided in the generation of the strong adhesive force that allows ivy to climb vertical surfaces.[4] Further study found that the ivy nanoparticles were less toxic than similarly sized TiO_2 and ZnO nanoparticles, which makes them an attractive candidate for UV fillers in sunscreens.[5] Similar organic nanostructures have been discovered in the secretions of a variety of marine species, including polychaetes, mussels, barnacles, and sea stars.[6] In fact, low-density lipoprotein (LDL) present in mammalian blood has long been recognized as a naturally occurring nanoparticle.[7] LDL serves as the main transport vehicle for cholesterol in mammalian systems, and bio-inspired LDLs have been used as potential carriers for targeted delivery of diagnostic and therapeutic agents.[8]

Most studies on naturally occurring organic nanoparticles have focused on higher organisms. Given the earth's rich biological diversity, it is reasonable to hypothesize that naturally occurring nanoparticles (NONPs), of various forms and functions, may be produced by a wide range of organisms from microbes to metazoans. In this study we have turned our focus to *Arthrobotrys oligospora*, a representative flesh eater with a saprophytic and predatory life stage in the fungal kingdom. In the presence of nematodes or proteinaceous substances, *A. oligospora* can change from a saprophyte into a predatory stage, characterized by the formation of 3D adhesive trapping networks that can trap nematodes for subsequent digestion.[9] The broad adaptability and flexible lifestyle of the fungus makes it an attractive

Dr. Y. Wang, L. Sun, S. Yi, Y. Huang,
Dr. S. C. Lenaghan, Prof. M. Zhang
Nano Bio-systems and Bio-Mimetics Lab
Department of Mechanical
Aerospace and Biomedical Engineering
The University of Tennessee
408 Dougherty Hall
1512 Middle Drive, Knoxville
TN 37996, USA
E-mail: mjzhang@utk.edu

DOI: 10.1002/adfm.201202619

candidate for the control of parasitic nematodes in both plants and animals.[10] Several biopolymers from the 3D-trapping networks of *A. oligospora* have been reported, and it is believed that both proteins and carbohydrates are involved in the adhesion process.[11]

Investigations of NONPs will not only help us to understand the roles of nanoparticles in biological systems, but also provide insight into the development of these nanomaterials for applications in biomedicine and biotechnology. In recent years, engineered nanomaterials have been crucial to the development of more effective cancer therapy and detection.[12] In cancer treatment, nanoparticles have shown promise by selectively taking advantage of the fundamental changes in morphology associated with oncogenesis.[13] Engineered nanoparticle-based delivery systems have displayed significant antitumor properties, and potential in chemotherapy, immunotherapy, radiotherapy, thermotherapy, and photodynamic therapy.[12] In this respect, NONPs, with near endless diversity, may be approached in the same way as other engineered colloidal particles that have been used for the above purposes. Understanding how these nanomaterials are formed in the natural system may also provide a template for the synthesis of "next generation" engineered or biomimetic nanostructures.

The purpose of this research was to discover new nanoparticles that occur naturally in *A. oligospora* and exploit their potential biomedical applications. Unlike higher organisms, microorganisms themselves are on the micrometer-scale. The colonial growth, development and appearance of microorganisms are largely susceptible to environmental parameters such as culture method, nutrients, and temperature. As a result, the possible interferences from the medium components/ingredients, especially the particle-based components present in solid medium, add a degree of complexity for more sophisticated designs to discover the NONPs formed inside or secreted from living microbial cells. Therefore, a proper culture system for discovering NONPs from microbial cultures without possible interfering from the culture medium is crucial to allow this type of study to be realized. In this study, a new culture method, fungal sitting drop culture method, was established that made it possible to observe fungal growth, as well as both secreted and surface-bound nanomaterials using light microscopy, scanning electron microscopy (SEM), and atomic force microscopy (AFM) without any disturbance from agar components present in solid media. Using this culture method, we observed secreted nanoparticles, and characterized these nanoparticles using SEM, AFM, and dynamic light scattering (DLS). We further analyzed the potential for these nanoparticles to be used as immunostimulatory agents, antitumor agents, and drug delivery carriers for cancer therapy.

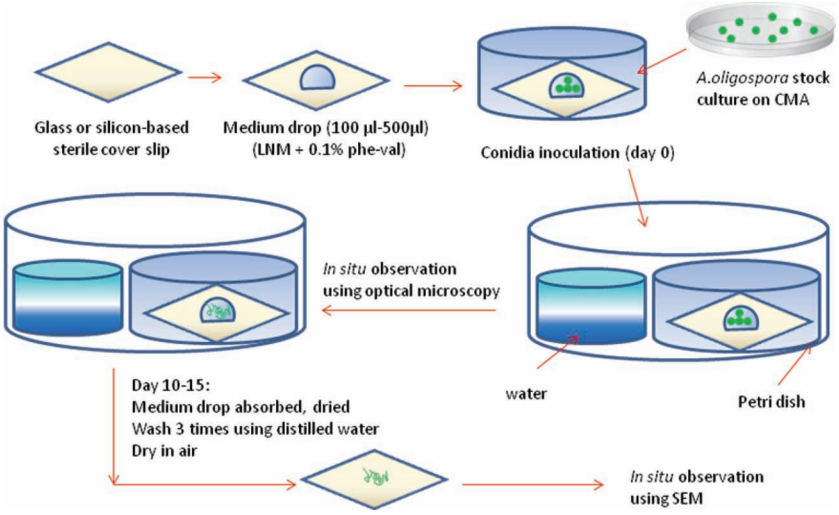

Figure 1. Illustration of a new fungal sitting drop culture method developed in this work. Briefly, a drop of medium was added onto a sterile cover slip and placed into a small Petri dish (3 cm), and then 50–100 conidia of *A. oligospora* from a stock culture on CMA dish were inoculated into the drop. Humidity was maintained by filling a second small Petri dish with water, and placing both into a large Petri dish (10 cm). The low nutrient medium (LNM) supplemented with 1 mg/mL phe-val was used as a liquid drop for fungal growth. The drop culture system was incubated at 25 °C for 15 days until the secreted nanoparticles were harvested.

2. Results and Discussion

2.1. Abundant Mycelia and 3D traps Development Using a Fungal Sitting Drop Culture System

A new fungal sitting drop culture method was first established as shown in **Figure 1**. A drop of medium was added onto a sterile cover slip and placed into a small Petri dish (3 cm). Humidity was maintained by filling a second small Petri dish with water, and placing both into a large Petri dish (10 cm). 50–100 conidia of *A. oligospora* from a stock culture on CMA dish were then

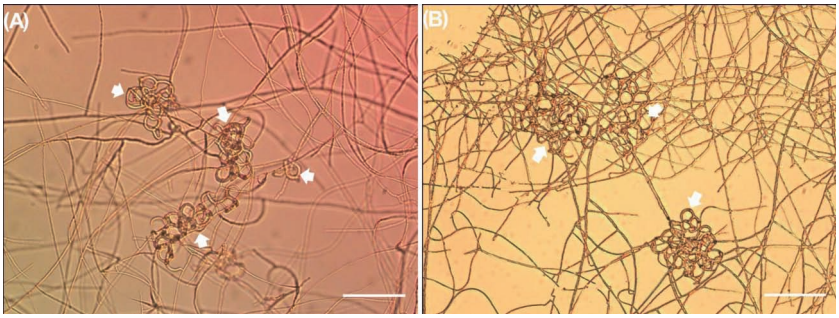

Figure 2. Abundant growth of *A. oligospora* mycelia and 3D traps in the novel sitting drop culture system was monitored in situ using inverted optical microscopy. A) *A. oligospora* growth in a medium drop on the cover slip on day 5 after inoculation; B) The air-dried *A.oligospora* mycelia with 3D traps on the cover slip on day 5 after inoculation. The liquid LNM supplemented with 1 mg/mL phe-val was used. Arrow indicates the 3D traps. Scale bars represent 200 µm.

inoculated into the drop and incubated at 25 °C. Germination took place during the first 24 h after inoculation, and after 3–4 days the first adhesive loop with diameter of 20–30 μm on the parent hyphae was observed. After this initial event, adhesive trap networks, consisting of one to several loops attached to each other in a 3D conformation, began to develop on the thin mycelium. The filamentous mycelium gradually grew to form a thick layer and the 3D traps increased both in size and number over a 5–15 day period. **Figure 2** shows images of the filamentous mycelia of *A. oligospora* and 3D traps in both a hydrated and dehydrated state at day 5 after inoculation.

In general, the sitting drop culture system developed here was derived from the hanging drop culture method for mammalian cell culture[14] and the fungal slide culture method.[15]

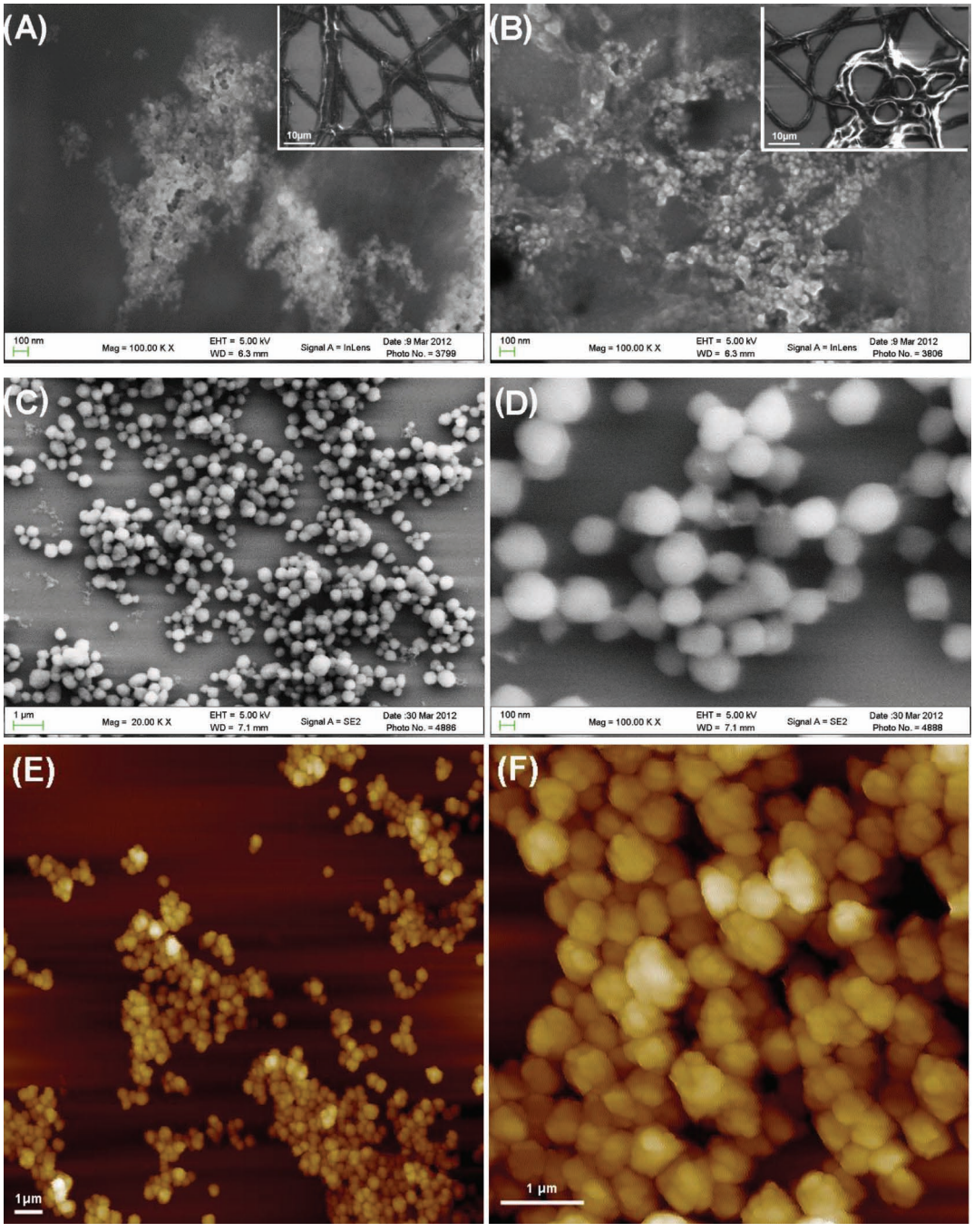

Figure 3. SEM/AFM images of nanoparticles generated from *A. oligospora* cultured in the drop culture system. A,B) Nanoparticles observed in situ on the surface of hyphae (A), and the 3D traps (B) of *A. oligospora* using SEM on the silicon wafer on which *A. oligospora* were cultured in a drop culture system. The inserts showed SEM image of partial hyphae (A) and partial 3D traps (B). C,D) SEM images of nanoparticles NONP-W prepared by washing the fungal mycelia; E,F) AFM images of nanoparticles NONP-W prepared by washing the fungal mycelia.

In this study, the low nutrient medium (LNM, Supporting Information Table S1) supplemented with 1 mg/mL phe-val was used as the media for fungal growth. It only includes five inorganic salts, two vitamins and one dipeptide, which prevented any particle contamination from the agar components present in solid media. In addition, the fungus used here is aerobic and generally needs aeration or bubbling when using conventional liquid culture method;[16] however, the drop volume used in this system was 100–500 µL, which allowed for significant gas exchange. Therefore this culture system is capable of growing fungal mycelia without any aeration or bubbling, and is adaptable for any aerobic fungal species. More importantly, because the fungus was cultured in a drop of media on a cover slip, we could monitor the growth of the fungus using optical microscopy in situ and even the secreted biomaterials using SEM or AFM.

2.2. Secreted Nanoparticles Observed Using SEM and AFM and their Characteristics

In order to observe the secreted and surface-bound nanomaterials from the filamentous mycelia or 3D traps using SEM, a silicon substrate was used to replace the glass cover slip in the drop culture system (Figure 1). On day 15 after inoculation, the media was removed from the silicon substrate on which the mycelia with 3D traps had developed. The sample was then washed three times using distilled water, air-dried, and imaged by SEM. As shown in **Figure 3**A,B, abundant nanoparticles were observed on the surfaces of the hyphae and 3D traps. Additionally, some nanoparticles were observed on the surface of the silicon substrate. After observation of the nanoparticles, the nanoparticles were collected by either washing the fungal mycelia with distilled water or by sonicating the mycelia in distilled water. In order to remove the impurities from the culture medium ingredients and other potential small molecules secreted from the fungus, the nanoparticles were further purified by dialysis for 3 days against distilled water using a 300 KDa cellulose acetate dialysis membrane. As shown in Figure 3C,D, the nanoparticles prepared by washing, NONP-W, had a diameter of 200–300 nm and were spherical in shape when analyzed by SEM. AFM revealed a similar finding, with nanoparticles ranging from 300–500 nm in diameter (Figure 3E,F). The nanoparticles prepared through sonication, NONP-S, were not significantly different from the washed nanoparticles.

Apart from the SEM and AFM observations, the particle size and zeta potential of the NONPs in solution were measured using DLS and Zeta Potential analysis. The NONP-W and NONP-S samples had an average size of 360–370 nm, with a zeta potential of –33 mV at pH 6.0 (**Table 1** and **Figure 4**). The chemical components of the NONPs were further analyzed by quantifying the glycosamnioglycan (GAG) and protein concentration in lyophilized NONPs. As shown in Table 1, there were ≈28 µg of GAG and ≈550 µg of protein in 1 mg of lyophilized nanoparticles. In addition, SDS-PAGE analysis confirmed that there were two main proteins with MWs of 110 and 80 KDa in both nanoparticle samples (Supporting Information Figure S2). As is well-known, GAGs are unbranched polysaccharides composed of repeating units of alternating uronic acids and amino sugars,[17] and carboxylic acid and sulphate groups that are deprotonated at physiological pH can give GAGs very high negative charge densities.[18] Therefore, negative zeta potential of the fungal NONPs were presumably, at least partially, resulted from the GAG component. Due to 3 Day dialysis with a 300 KDa dialysis membrane, free protein components with low MWs in the samples should be completely removed. Therefore, two proteins with respective MWs of 110 and 80 KDa found in both NONP samples should be structural components in the fungal NONPs. Since most glycosaminoglycans are covalently attached to core proteins to form proteoglycans,[17] we presume that two protein components probably were covalently attached to the GAGs in the fungal NONPs.

Table 1. Characteristics of the naturally occurring nanoparticles (NONPs) from *A. oligospora* and NONP-DOX conjugates.

	Particle Size [nm]	Zeta Potential [mV]	GAG [µg/mg]	Protein [µg/mg]
NONP-W [a)]	371.2 ± 74.59	–33.2 ± 5.55	28.03 ± 1.32	544.73 ± 16.70
NONP-S [b)]	369.0 ± 67.49	–33.9 ± 5.77	28.22 ± 5.39	554.42 ± 22.93
NONP-DOX [c)]	380.9 ± 60.13	–20.8 ± 5.37	–	–

[a)]NONP-W: the nanoparticles prepared by washing the mycelia on the cover slip using distilled water; [b)]NONP-S: the nanoparticles prepared by sonicating the mycelia in distilled water; [c)]NONP-DOX: the conjugates between NONP-W and antitumor drug, DOX (doxorubicin), via amide linkages.

2.3. Secreted Nanoparticles Are Not Related to 3D-Trap Formation, but to the Growth of Mycelia

Currently, little is known about how the nanoparticles are secreted from this fungus and what biological functions they play during the growth and development of the fungus. However, we tested the possible source of the secreted nanoparticles in this study. For this purpose, different media were used in the drop culture system, and the amounts of nanoparticles produced were compared. As shown in **Table 2**, when the LNM was supplemented with 1 mg/mL phe-val, the predatory stage of the fungus developed, resulting in abundant 3D adhesive traps (Figure 2). There was ≈8.39 µg GAG produced by one cover slip on which 0.5 mL of medium, i.e., LNM + dipeptide, was added. According to Table 1, there was ≈28 µg GAG per mg of NONPs. Thus, ≈0.6 mg NONPs was produced per mL of the medium (LNM + dipeptide) after 15-day culture of *A. oligospora*. When the LNM was supplemented with 12 mM phosphate buffer, only the saprophytic stage of the fungus developed, resulting in comparable mycelia growth without trap formation. However, the nanoparticles produced from the above two media did not show significant differences in GAG concentration. In the case of the LNM without phe-val, the fungus developed sparse 3D traps, but abundant hyphae growth. It also produced the comparable amount of the nanoparticles compared to the LNM with phe-val or phosphate buffer. However, when LNM/phe-val was initially used as the medium, and then changed to pure water, the 3D

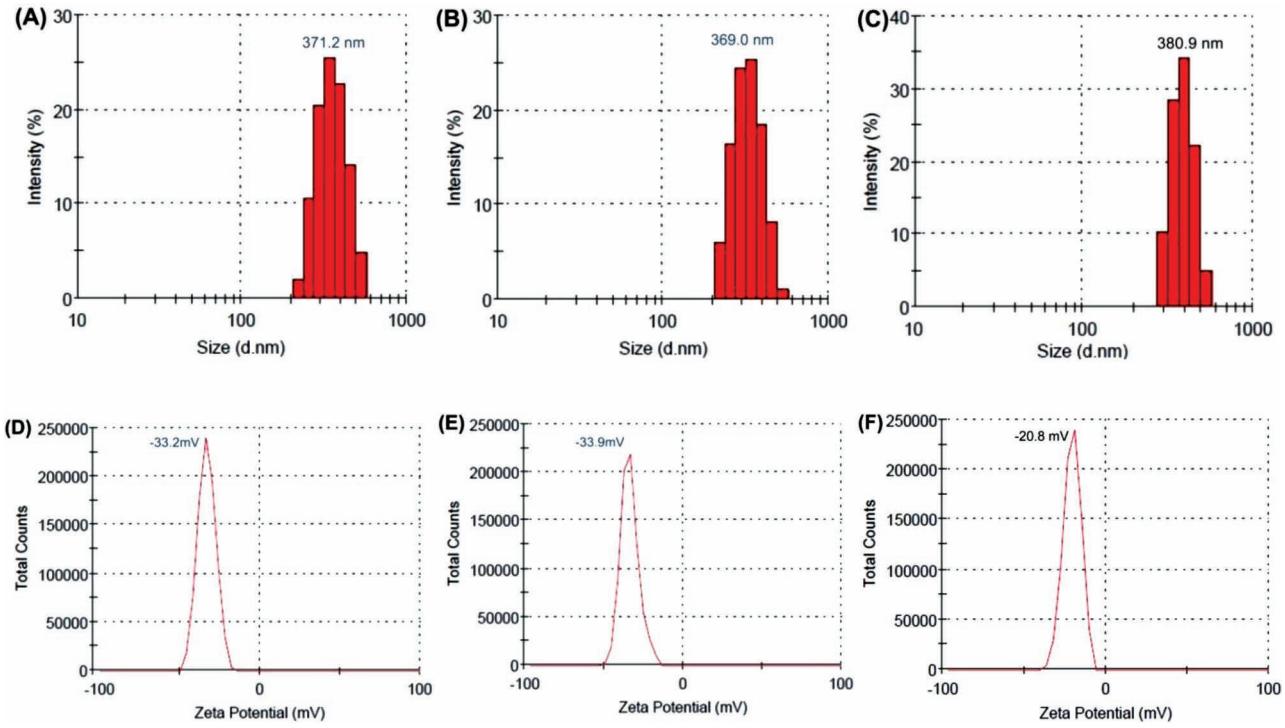

Figure 4. Average particle sizes and zeta potentials of the naturally occurring nanoparticles (NONPs) from *A. oligospora* and the NONP-DOX (DOX = doxorubicin) conjugates. The particle size and zeta potential of the A,D) sample NONP-W, B,E) sample NONP-S, and C,F) the sample NONP-DOX conjugates were measured using a DLS method. The average particle sizes of both NONPs were ≈360–370 nm, and there were no significant differences in size for the NONP-DOX conjugates compared to both NONPs. However, the zeta potential for the NONP-DOX conjugates increased to –20 mV from –33 mV of unconjugated NONPs.

traps and hyphae developed in the drop culture system were less sparse than using LNM/pha-val medium. Accordingly, the fungus produced fewer amounts of nanoparticles. If only water was used as a medium, the fungus grew slowly, producing the fewest hyphae and no traps. Consequently these samples had the fewest amount of nanoparticles. Based on this data, it can be concluded that the NONPs secreted from *A. oligospora* were not related to 3D trap formation, but instead to the growth of mycelia.

Table 2. The effect of 3D traps, mycelia and medium ingredients on the nanoparticle secretion from the fungus.

	3D traps[a)]	Mycelia[a)]	Nanoparticles [GAG, μg][b)]
LNM + dipetide	+++	+++	+++ (8.39 ± 0.15)
LNM + PO^{4-}	–	+++	+++ (8.44 ± 0.27)
LNM	+	+++	+++ (8.21 ± 0.11)
LNM + dipetide (Initial media)/ water (subsequent replenishment)	+	++	++ (6.17 ± 0.34)
Water	–	+	+ (2.14 ± 0.05)

[a)]The amount of 3D traps and mycelia observed by optical microscopy. The fungus was cultured in sitting drop culture system in which 0.5 mL medium was added on a cover slip, and the experiments were performed in triplicate; [b)]The GAG amounts stand for the amount of the nanoparticle produced by one cover slip on which 0.5 mL medium was added. The experiments were performed in triplicate.

2.4. Immunostimulatory Effect of the NONPs on RAW 264.7 Mouse Macrophages

Significant experimental evidences suggest that some polysaccharides from higher plants, mushrooms, lichens and algae possess an immunostimulatory activity both in vivo and in vitro.[19] Some GAGs, such as heparin, heparan sulfate, chondroitin sulfate and their mimetics, have also been reported as potential cancer therapeutics, inhibiting tumor cell adhesion, migration, growth, and invasion in vitro.[17] Other proteoglycans formed by covalently attaching GAGs to core proteins, such as decorin, seem to be effective potential therapeutics that reduced primary tumor growth by 70% and eliminated metastases in an orthotopic mammary carcinoma model.[20] Inspired by these studies, we tested the potential immunostimulatory effect and cytotoxic effect of the NONPs in vitro. The immunostimulatory potential of the NONP-W and NONP-S samples was first tested on RAW 264.7 macrophages using dose-titration (0.5–25 μg/mL) assays. **Figure 5**A shows the TNF-α concentration in the culture media of RAW264.7 cells treated with the nanoparticles for 24 h. In both cases, NONP-W and NONP-S, the RAW264.7 cells secreted significantly greater

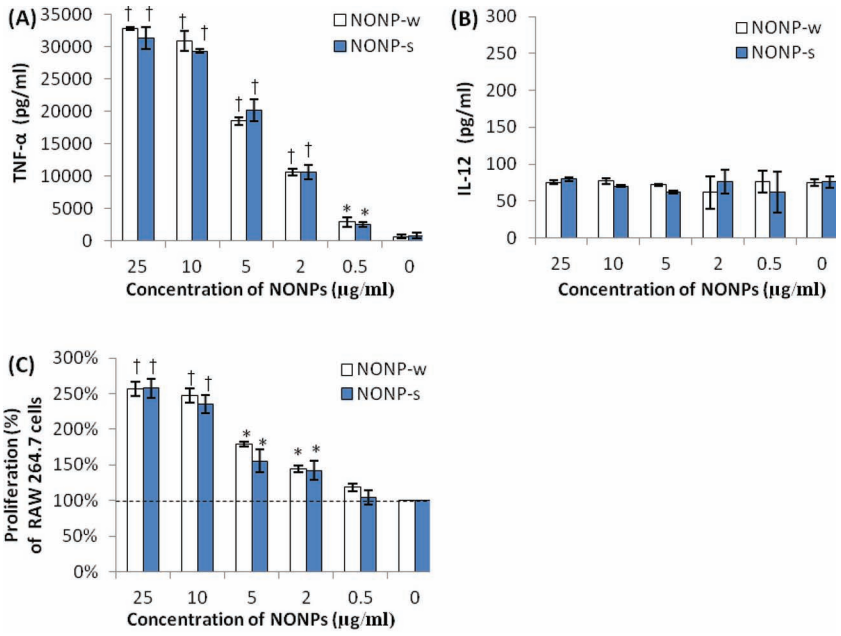

Figure 5. Effects of NONPs from *A. oligospora* on the production of TNF-α, and IL-12 in RAW 264.7 macrophage cells. A) Dose dependent TNF-α induction from RAW cells by NONPs from *A. oligospora*; B) NONPs from *A. oligospora* did not induce IL-12 production from the cells. C) Dose- dependent proliferation of RAW cells by NONPs from *A. oligospora*. The cells were treated with NONP-W or NONP-S at various concentrations. The supernatant were then collected and measured at 24 h after addition of each sample. The proliferation rate was measured using the MTT assay after removing of the cytokine-containing supernatant at 24 h after incubation. Results are expressed as the mean ± SD. $*P < 0.05$, $\dagger P < 0.01$, significantly different from the control.

amounts of TNF-α (about 3- to 39-fold) than the control treatment, in a dose-dependent manner. There were no significant differences in TNF-α induction between the NONP-W and NONP-S samples. As is well-known, macrophages are the first cells to recognize invading foreign bodies and are central to cell-mediated and humoral immunity.[19c,21] The elevated secretion of cytokines, such as TNF-α, IL-6 and IL-12, from activated immune cells trigger other immune cells through various receptors.[22] Although no significant induction in IL12 secretion was observed from the activated macrophages (Figure 5B) in this study, the elevated secretion of TNF-α indicates that the NONPs from this fungus possess potential immunostimulatory effects.

At the same time, examination of the cytotoxicity of the NONPs against RAW 264.7 macrophages by the MTT assay indicated that there was no cytotoxicity on RAW 264.7 macrophages. On the contrary, besides the macrophage-activating effects mentioned above, the NONPs unexpectedly enhanced the proliferation of RAW 264.7 macrophages in a dose-dependent manner at all concentrations examined during the 24 h incubation (Figure 5C). It was previously reported that TNF-α has no proliferation effects alone but decreases significantly the population doubling time for mouse macrophages stimulated by macrophage colony stimulating factor.[23] Although it is still not clear if the proliferation effect of RAW 264.7 macrophages was attributed to the evaluated TNF-α secretion, the increased proliferation of the macrophages will aid the modulation of macrophage immune function in vivo.[19c]

2.5. In vitro Cytotoxicity of the NONPs and the NONP-DOX Conjugates Against Tumor Cells

Apart from the evaluation of potential immunostimulatory activity, the cytotoxic effect of the nanoparticles was then investigated using human non-small-cell lung cancer A549 cells and murine melanoma B16BL6 cells. As shown in **Figure 6**A,B, both NONP samples showed dose-dependent cytotoxicity on both tumor cell lines after 48-h incubation. At a concentration of 2 μg/mL, the NONPs only inhibited cell proliferation by 5–10%, and no significant differences were seen at that concentration compared to the blank control; however, at a concentration of 100 μg/mL, 35–45% inhibition rates were significantly observed for both cells. According to this data, the IC_{50} of the NONPs for both tumor cell lines was estimated to be greater than 100 μg/mL, suggesting that the NONPs had only a slight cytotoxic activity compared to some cytotoxic antitumor drugs.

Even though the nanoparticles themselves have only a minimal cytotoxic activity, they could still be a potential candidate for tumor therapy, especially when conjugated with certain antitumor drugs. For this purpose, we tested if the fungal NONPs can function as a potential drug carrier by conjugating the antitumor drug doxorubicin (DOX) to the nanoparticles in vitro. Due to the existence of GAGs in the nanoparticles, we assumed that there were carboxyl and sulphate groups on the nanoparticles. DOX was then conjugated to these carboxyl groups of NONP-W via amide linkages (Supporting Information Figure S1). The bioconjugation efficiency for the NONP-DOX conjugates was 29% under current reaction conditions (see the Experimental Section). The average nanoparticle size of NONP-DOX was ≈380 nm, and there were no significant differences in size for the NONP-DOX conjugates compared to both NONPs. However, the zeta potential for the NONP-DOX conjugates increased to –20 mV from –33 mV observed in unconjugated NONPs (Figure 4C,F). The FTIR spectra of NONP-W before and after conjugation to DOX were also characterized (Supporting Information Figure S3). As shown in Figure 6C,D, the NONP-DOX conjugates showed higher inhibitory effects on both cells in dose-dependent manners, compared to free DOX. The IC_{50} values for NONP-DOX conjugates and free DOX listed in **Table 3** demonstrate a synergistic cytotoxic effect when DOX was conjugated to the NONPs. At an IC_{50} of free DOX for both cells (≈254 nM for B16BL6, and ≈552 nM for A549), the free DOX inhibited cell proliferation by 50%, whereas the NONP-DOX conjugates showed 61% and 68% inhibition against the A549 and B16Bl6 cells, respectively. According to the bioconjugation efficacy (29%), the concentration of NONP-W in the NONP-DOX conjugates at the respective IC_{50} of free DOX for the A549 and B16Bl6 cells was calculated to be around 0.51 and 1.1 μg/mL; however, almost no significant inhibition effect on both cells was observed at that concentration for nanoparticles

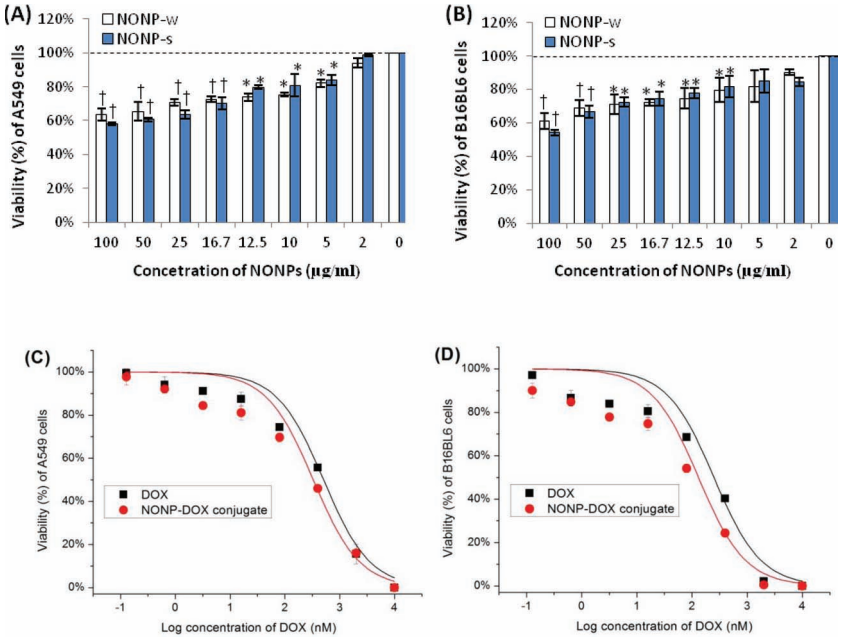

Figure 6. In vitro cytotoxocity of the NONPs or the NONP-DOX conjugates against A,C) human non-small-cell lung cancer A549 cells and B,D) mouse melanoma B16BL6 cells. Both tumor cells were treated with nanoparticles at the concentration range of 2–100 μg/mL or with the NONP-DOX conjugates at the DOX concentration range of 0.1 nM to 10 μM for 48 h. The inhibitory effects of both samples, NONP-W and NONP-S, on both cells in dose-dependent manners were observed at the NONP concentration examined. The sigmoidal dose-response curves were fitted and the concentration of NONP-DOX conjugates and free DOX that inhibited cell survival by 50% (IC_{50}) was determined from cell survival plots using "DoseResp" function of OriginPro 8.0. ∗P < 0.05 and †P < 0.01, as compared with the blank control.

themselves (Figure 6A,B). This indicates that NONP and DOX in the conjugated nanoparticles exerted synergistic cytotoxic effects, which led to the IC_{50} values 1.6–1.8 fold lower in A549 cells and B16BL6 cells (Table 3).

2.6. Cellular Uptake and Intracellular Distribution of the NONP-DOX Conjugates in Tumor Cells

Apart from the cytotoxicity assay, the cellular uptake and intracellular distribution of NONP-DOX conjugates, containing 10 μM DOX, for both cell lines was further examined using flow cytometry and confocal microscopy, respectively. As shown in **Figure 7**, after a 4-h incubation, there was no significant difference in the DOX fluorescence for free DOX and NONP-DOX conjugates at a DOX concentration of 10 μM. To further observe sub-cellular distribution of NONP-DOX conjugates, the nuclei and endosomes/lysosomes (endolysosome) were labeled with the nucleus-selective dye (Hoechst 33342, blue) and acidic endolysosomes-selective dye (LysoTracker green DND-26), respectively. As shown in **Figure 8**, different intracellular distribution of NONP-DOX conjugates and free DOX was observed in both cells after a 4-h treatment. Majority of DOX in both cells treated with NONP-DOX conjugates were predominantly located in the endosomal/lysosomal compartment, whereas most of the free DOX was located outside endolysosomes. Since major nanoparticles internalized via endocytosis were typically found mainly within endosomes or lysosomes,[24] it is likely that the NONP-DOX conjugates might be taken up by endocytic pathway in both tumor cell lines. In addition, a small fraction of DOX was seen in the nucleus of B16BL6 cells treated with free DOX, whereas the treatment of NONP-DOX conjugates did not result in obvious nuclear distribution (Figure 8B). In the case of A549 cells, no significant DOX fluorescence was seen in the nucleus for both treatments (Figure 8A). No obvious DOX localization in nucleus of A549 cells treated with free DOX during 4-h incubation was consistent with the previous

Table 3. IC50 values [nM] of NONP-DOX conjugates and free DOX on melanoma and lung cancer cells (48 h).

	Lung cancer A549 cells	Melanoma B16BL6 cells
Free DOX	551.71 ± 36.72	254.22 ± 11.35
NONP-DOX conjugates	342.34 ± 57.17∗	139.93 ± 28.30∗
NONP ctrl	>100 μg/mL	>100 μg/mL

IC_{50} was determined from cell survival plots using "DoseResp" function of OriginPro 8.0; ∗P < 0.05, as compared with free DOX.

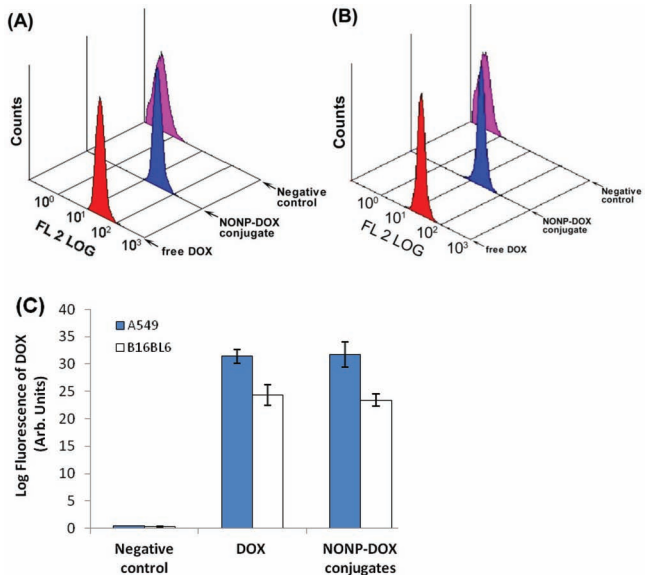

Figure 7. Flow cytometry analysis for cellular uptake of NONP-DOX conjugates in A) human lung cancer A549 cells and B) mouse melanoma B16BL6 cells. Both cells were treated with NONP-DOX conjugates or free DOX at DOX concentration of 10 μM for 4 h, and then the mean DOX fluorescence associated with the cells were measured by collecting 20 000 events for each sample. C) Statistical analysis of the mean DOX fluorescence associated with the cells was compared, and no significant differences between DOX and NONP-DOX conjugates were observed for respective cell line.

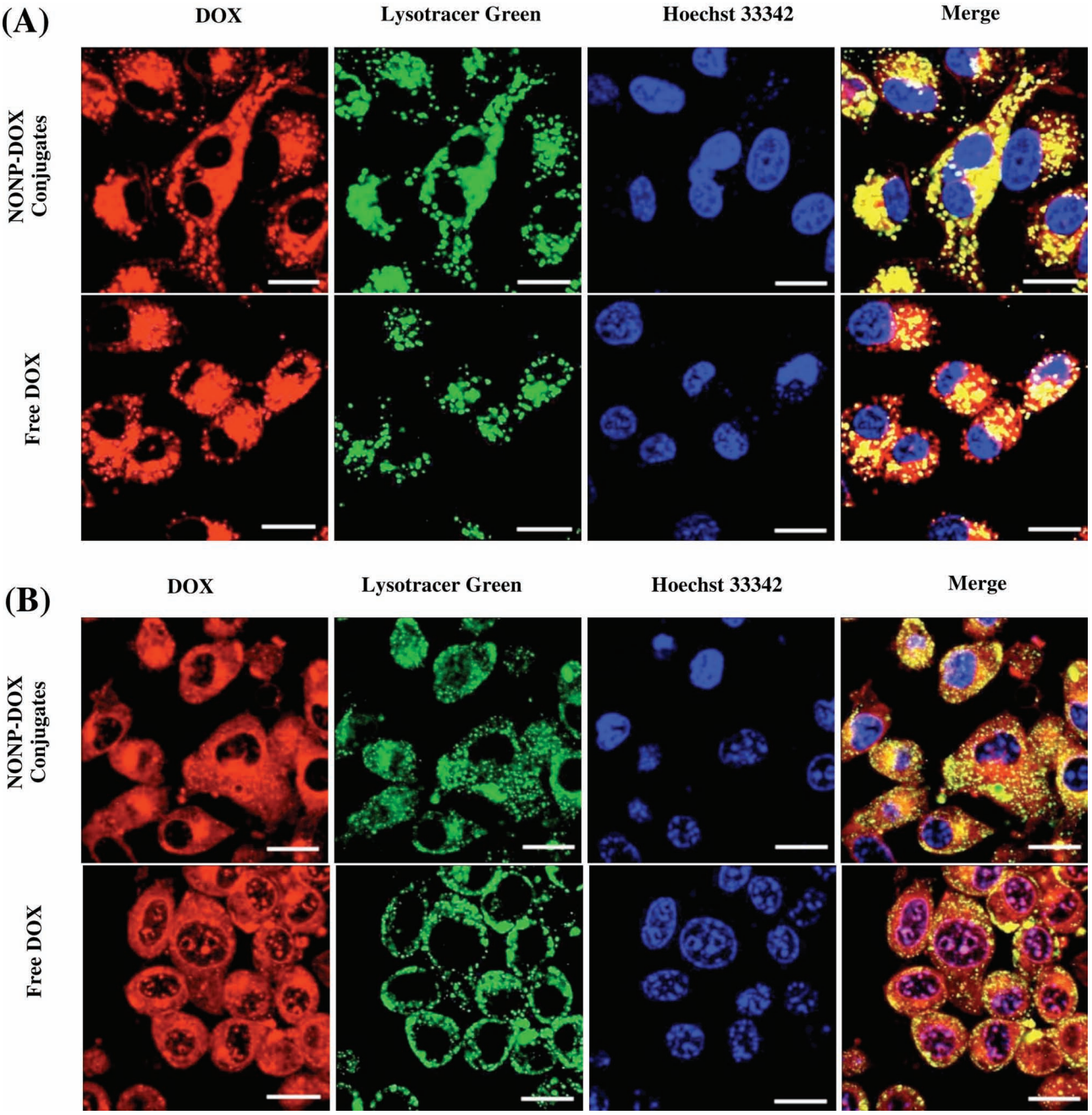

Figure 8. Intracellular distributions of NONP-DOX conjugates and free DOX at the DOX concentration of 10 μM in A) human lung cancer A549 cells mouse and B) mouse melanoma B16BL6 cells. The cells were incubated with the samples at 37 °C, 5% CO_2 for 4 h, and then 100 nM Lysotracer Green DND-26 and 4 μM Hoechst 33342 were added for 30 min incubation prior to visualization by confocal microscopy. Scale bars represent 10 μm.

results,[25] presumably due to diverse drug responses in different types of cells. However, no obvious nuclear distribution in both cells treated with NONP-DOX conjugates was likely resulted from the sequestration of the conjugates in the endolysosomal compartments during 4-h incubation.[26] Overall, the results here demonstrate that even though there was a different subcellular distribution, conjugation of DOX to NONPs did not decrease DOX uptake by both tumor cell lines (Figure 7).

3. Conclusion

A new culture method, fungal sitting drop culture method, was established in order to monitor the growth of *A. oligospora* in situ, and observe the nanoparticle production without interfering or contamination from the solid media. Abundant spherical nanoparticles secreted from the fungus were first revealed by scanning electron microscopy and atomic force microscopy. It was then confirmed that the NONPs secreted from *A. oligospora*

were not related to the formation of the 3D traps, but instead were secreted from growing mycelia. Further analyses revealed that the fungal NONPs had an average size of 360–370 nm, with a zeta potential of –33 mV at pH 6.0. They contained ≈28 μg of glycosaminoglycan and ≈550 μg of protein per mg of nanoparticles. Interestingly, the NONPs from *A. oligospora* have demonstrated potential capability as an immunostimulatory and antitumor agent. They significantly induced TNF-α secretion in RAW264.7 mouse macrophages, showed slight cytotoxicity to mouse melanoma B16BL6 and human lung cancer A549 cells, and demonstrated a synergistic cytotoxic effect upon conjugation with DOX against both cells. Therefore, they may play multifunctional roles as a promising candidate for potential tumor immunochemotherapy. In this respect, the synergistic antitumor efficacy for chemotherapy, drug delivery and immune regulation are expected in vivo. More importantly, this study has proposed a new approach for producing novel organic nanoparticles from microorganisms under controllable conditions. It may open up a new avenue for controlling the synthesis of organic nanoparticles using synthetic biology in the future.

4. Experimental Section

Chemicals, Fungus and Cell Line: Arthrobotrys oligospora (ATCC 24927), RAW 264.7 murine macrophages (TIB-71) and A549 human non-small-cell lung cancer cells (CCL-185) were obtained from the American Type Culture Collection (Manassas, VA). The B16BL6 murine melanoma cell line was obtained from the National Cancer Institute-Central Repository (Frederick, MD). Corn Meal Agar (CMA), phe-val, thiamin-HCl, biotin, doxorubicin hydrochloride, and PBS were purchased from Sigma-Aldrich (St. Louis, MO). LysoTracker Green DND-26 and Hoechst 33342 were obtained from Invitrogen Life Technologies (Grand Island, NY). Fetal bovine serum and DMEM medium were purchased from Mediatech (Manassas, VA). Penicillin (10 000 units/mL)-streptomycin (10 000 μg/mL) solution was procured from MP biomedicals (Solon, OH).

Fungal Culture in the Sitting Drop Culture System: Freeze-dried *A. oligospora* was first inoculated into CMA medium (pH 7.0) and incubated at 25 °C for 3–10 days, resulting in mycelia development and sufficient conidia production. The conidia were collected from the above stock cultures using Tween-80 (0.02%), and aliquots of the conidia suspension were stored at –20 °C. The sitting drop culture method was developed as shown in Figure 1. Conidia suspension (about 50–100 conidia in 10 μL) was inoculated into the media droplet and incubated at 25 °C for 3–15 days. A modified low nutrient medium (LNM)[10c] was used in this work for the fungal drop culture, and its ingredients are listed in Supporting Information Table S1. In the case of testing the possible source of the secretory nanoparticles from the fungus, other media ingredients were also used. For instances, the LNM supplemented with 1 mg/mL phe-val was used to grow the predatory stage of the fungus (formation of 3D adhesive capture traps), or supplemented with phosphate buffer (12 mM)[11] for growth of the saprophytic stage of the fungus (only mycelia growth without trap formation). In experiments testing the effect of LNM ingredients on the nanoparticle secretion, distilled water (pH 7.0) was also used to completely or partially replace the LNM.

Sample Preparation and Nanoparticle Characterization: 50–100 conidia were inoculated into the sitting drop culture system described above, and incubated at 25 °C for 3–15 days. The fungal hyphae development and the formation of 3D traps were monitored in situ using optical microscopy. After a 15-day incubation, the media was removed, and the mycelia on the silicon-based cover slip were gently washed using distilled water, and then air-dried for SEM (LEO 1525, high resolution FE-SEM system, Germany). To prepare the secreted nanoparticles from the fungal culture, the mycelia on the cover slip were first washed 10 times using distilled water (1 mL), and the wash water was collected and designated as sample NONP-W. The washed mycelia on the cover slip were also collected in 1 mL distilled water and then were sonicated in a water-bath sonicater (model 750D, VWR) at RT for 30 min. The sonicated sample was spun down at 1000 rpm for 5 min and the supernatant was collected and designated as sample NONP-S. Both sample NONP-W and NONP-S were filtered through a 1-μm syringe filter (Nylon membrane, Whatman, Florham Park, NJ) and then dialyzed using CE dialysis tubing (molecular weight cut-off: 300 kDa, Spectrum Labs, CA) against distilled water for 3 days. Both dialyzed NONP-W and NONP-S (10 μL) were then transferred onto silicon wafers, dried and directly examined using SEM. The nanoparticles were also visualized using an Agilent 6000 ILM/AFM atomic force microscope (Agilent Technologies, Santa Clara, CA) by placing and air-drying the samples (10 μL) on glass cover slips. The operation was performed in AC mode, using an ACTA Probe from AppNano (Santa Clara, CA) controlled with the Picoview software package. Particle size, size distribution and zeta potential of the dialyzed NONPs were further determined at 25 °C using a Malvern Zetasizer, NANO ZS (Malvern Instruments Limited, UK), with a He-Ne laser (wavelength of 633 nm) and a detector angle of 173°. All samples were measured in triplicate.

Determination of Glycosaminoglycan and Protein in NONPs: To determine the presence of glycosaminoglycan and protein in the nanoparticles, the dialyzed NONP-W and NONP-S samples were lyophilized and weighed. The amount of sulfated glycosaminoglycans in the samples was quantified using a Proteoglycan Detection Kit (1,9-dimethylmethylene blue, Astarte Biologics, Redmond, WA) according to the manufacturer's procedure. Similarly, the concentration of protein in the samples was quantitatively determined using the BCA Kit (Pierce, Rockford, IL) according to the the manufacturer's protocol.

In Vitro Immunostimulatory Activity: The mouse macrophage cell line, RAW264.7, was used to measure the potential immunostimulatory effect of the nanoparticles.[22,27] Briefly, the RAW 264.7 cells were grown in DMEM medium supplemented with heat-inactivated FBS (10%) and penicillin-streptomycin (1%) at 37 °C. The cells were then seeded onto 12-well culture plates at a density of 5×10^6 cells/mL and cultured for 24 h. The cells were then washed three times with PBS (0.5 mL), before addition of NONP-W and NONP-S samples at various concentrations. After addition of the test samples, the cells were incubated for 24 h, and the supernatants were collected and stored at –20 °C. The levels of TNF-α and IL-12 in the supernatants were determined by enzyme-linked immunosorbent assay (ELISA) using an OptEIA ELISA Set (BD, San Jose, CA).

Synthesis of NONP-Doxorubicin Conjugates: Conjugation of DOX to the nanoparticles through amides bond between the 3′-amine of DOX and the free carboxyl groups of the nanoparticles was achieved using DEC and sulfo-NHS as the coupling agents[28] (Supporting Information Figure S1). Briefly, the nanoparticles (0.1 mg) were dissolved in water (0.5 mL) and mixed with EDC (0.4 mg) and sulfo-NHS (0.1 mg). The solution was incubated at ambient temperature for 30 min to modify the carboxyl groups of the nanoparticles with sulfo-NHS. After that, DOX (0.26 mg) was added to the activated solution, and stirred overnight to complete the reaction. Finally, the resulting solution was poured into the CE dialysis tube (molecular weight cut-off: 300 kDa) and dialyzed against deionized water for 3 days. After lyophilization, the obtained NONP-DOX conjugate was characterized by FTIR analysis (Varian). Three replicates were carried out to assess the average DOX content in NONP-DOX conjugate and the bioconjugation efficiency (%). The particle size and zeta potential of NONP-DOX conjugates were also measured as described above.

MTT Assay: The MTT (3-[4, 5-dimethylthiazol-2-yl]-2, 5-diphenyl tetrazolium bromide) assay was utilized to assess cytotoxicity of the nanoparticles as previously reported.[29] Briefly, 1×10^4 tumor cells (melanoma B16BL6 and non-small-cell lung cancer A549) were seeded in 96-well plates in 100 μL DMEM. Serial dilutions of nanoparticles were added to the plate and incubated at 37 °C in 5% CO_2 for 48 h. MTT stock solution (10 μL, 5 mg/mL in PBS, pH 7.4) were then added into the wells and the plates were incubated at 37 °C for another 4 h. The

medium was then removed and DMSO (100 μL) was added to each well to solubilize the dye. The absorbance was measured using a microplate reader (Bio-Tek μQuant) at 570 nm, and the concentration of drug that inhibited cell survival by 50% (IC_{50}) was determined from cell survival plots using the "DoseResp" function of OriginPro 8.0.

Cellular Uptake and Confocal Microscopic Study: The cellular uptake of DOX was quantified according to the reported method.[30] Briefly, tumor cells were seeded into 6-well plates at densities of 1×10^6 cells/mL, and incubated at 37 °C until 70% confluence was reached. Free DOX solution or NONP-DOX conjugates at DOX concentration of 10 μM were then added and incubated for 4 h at 37 °C. The medium was aspirated and cells were rinsed with cold PBS three times. Flow cytometry analysis was immediately carried out on an Epics XL Analyzer (Beckman Coulter Inc., Brea, CA) by collecting 20 000 events for each sample and the cell associated fluorescence was measured. Each experiment was performed in triplicate. Confocal microscopy was used to investigate the intracellular distribution in the tumor cells treated with NONP-DOX conjugates and free DOX. The cells were grown on cover slips to 50% confluence and incubated with samples at DOX concentrations of 10 μM at 37 °C for 4 h. To observe the intracellular distribution of the DOX-loaded NONP, the cells were incubated with LysoTracker green (100 nM) and Hoechst 33342 (4 μM) for 30 min prior to visualization for endolysosome and nuclear labeling, respectively. The cells were then washed three times with PBS, and immediately imaged by a FluoView FV1000 Confocal Microscope (Olympus, Japan).

Statistical Analysis: The data were expressed as mean ± SD. Statistical significance was determined using a one-way ANOVA followed by a Student's t test for multiple comparison tests. A p value of <0.05 was considered as statistically significant.

Supporting Information

Supporting Information is available from the Wiley Online Library or from the author.

Acknowledgements

This material is based upon work supported by, or in part by, the U. S. Army Research Laboratory, the U. S. Army Research Office under contract/grant number ARO W911NF-10-1-0114.

Received: September 11, 2012
Revised: October 25, 2012
Published online: December 4, 2012

[1] M. R. Wiesner, G. V. Lowry, E. Casman, P. M. Bertsch, C. W. Matson, R. T. Di Giulio, J. Liu, M. F. Hochella, Jr., *ACS Nano* **2011**, *5*, 8466.
[2] a) M. F. Hochella, D. Aruguete, B. Kim, A. S. Madden, in *Nature's Nanostructures* (Eds: G. Haibo, B. Amanda), Pan Stanford Publishing, Victoria, Australia **2012**; b) L. Goldman, C. Coussens, *Implications of Nanotechnology for Environmental Health Research*, The National Academies Press, Washington DC, USA **2005**.
[3] a) S. B. R. Chang, J. L. Kirschvink, *Annu. Rev. Earth Planet. Sci.* **1989**, *17*, 169; b) J. L. Kirschvink, A. Kobayashi-Kirschvink, B. J. Woodford, *Proc. Natl. Acad. Sci. USA* **1992**, *89*, 7683; c) W. Wiltschko, U. Munro, R. Wiltschko, J. L. Kirschvink, *J. Exp. Biol.* **2002**, *205*, 3031.
[4] a) M. Zhang, M. Liu, H. Prest, S. Fischer, *Nano Lett.* **2008**, *8*, 1277; b) S. C. Lenaghan, M. Zhang, *Plant Sci.* **2012**, *183*, 206.
[5] L. Xia, S. Lenaghan, M. Zhang, Z. Zhang, Q. Li, *J. Nanobiotechnol.* **2010**, *8*, 12.
[6] a) L. J. Xia, S. C. Lenaghan, M. J. Zhang, Y. Wu, X. Zhao, J. N. Burris, C. N. Stewart, *J. Nanopart. Res.* **2011**, *13*, 1029; b) M. J. Stevens, R. E. Steren, V. Hlady, R. J. Stewart, *Langmuir* **2007**, *23*, 5045; c) M. Zhang, M. Liu, S. Bewick, Z. Suo, *J. Biomed. Nanotechnol.* **2009**, *5*, 294; d) M. Berglin, P. Gatenholm, *Colloids Surf., B* **2003**, *28*, 107; e) E. Hennebert, P. Viville, R. Lazzaroni, P. Flammang, *J. Struct. Biol.* **2008**, *164*, 108.
[7] a) I. R. Corbin, H. Li, J. Chen, S. Lund-Katz, R. Zhou, J. D. Glickson, G. Zheng, *Neoplasia* **2006**, *8*, 488; b) M. Rizzo, K. Berneis, *Q. J. Med.* **2006**, *99*, 1.
[8] a) H. Jin, J. F. Lovell, J. Chen, Q. Lin, L. Ding, K. K. Ng, R. K. Pandey, M. Manoharan, Z. Zhang, G. Zheng, *Bioconjug. Chem.* **2012**, *23*, 33; b) I. R. Corbin, G. Zheng, *Nanomedicine* **2007**, *2*, 375; c) J. D. Glickson, S. Lund-Katz, R. Zhou, H. Choi, I. W. Chen, H. Li, I. Corbin, A. V. Popov, W. Cao, L. Song, C. Qi, D. Marotta, D. S. Nelson, J. Chen, B. Chance, G. Zheng, *Mol. Imaging* **2008**, *7*, 101.
[9] Y. Yang, E. Yang, Z. An, X. Liu, *Proc. Natl. Acad. Sci. USA* **2007**, *104*, 8379.
[10] a) B. Nordbringhertz, B. Mattiasson, *Nature* **1979**, *281*, 477; b) J. K. Yang, L. Wang, X. L. Ji, Y. Feng, X. M. Li, C. G. Zou, J. P. Xu, Y. Ren, Q. L. Mi, J. L. Wu, S. Q. Liu, Y. Liu, X. W. Huang, H. Y. Wang, X. M. Niu, J. Li, L. M. Liang, Y. L. Luo, K. F. Ji, W. Zhou, Z. F. Yu, G. H. Li, Y. J. Liu, L. Li, M. Qiao, L. Feng, K. Q. Zhang, *PloS Pathog.* **2011**, *7*; c) B. Nordbrin, *Physiol. Plant.* **1973**, *29*, 223; d) X.-M. Niu, K.-Q. Zhang, Mycology **2011**, *2*, 59.
[11] A. Tunlid, T. Johansson, B. Nordbringhertz, *J. Gen. Microbiol.* **1991**, *137*, 1231.
[12] N. P. Praetorius, T. K. Mandal, *Recent Pat. Drug Delivery Formulation* **2007**, *1*, 37.
[13] L. Brannon-Peppas, J. O. Blanchette, *Adv. Drug Delivery Rev.* **2004**, *56*, 1649.
[14] S. W. Potter, J. E. Morris, *Anat. Rec.* **1985**, *211*, 48.
[15] J. L. Harris, *J. Clin. Microbiol.* **1986**, *24*, 460.
[16] E. Friman, S. Olsson, B. Nordbrighertz, *Fems Microbiol. Ecol.* **1985**, *31*, 17.
[17] G. W. Yip, M. Smollich, M. Gotte, *Mol. Cancer Ther.* **2006**, *5*, 2139.
[18] N. S. Gandhi, R. L. Mancera, *Chem. Biol. Drug Des.* **2008**, *72*, 455.
[19] a) B. S. Paulsen, *Curr. Org. Chem.* **2001**, *5*, 939; b) H. H. Lee, J. S. Lee, J. Y. Cho, Y. E. Kim, E. K. Hong, *J. Microbiol. Biotechnol.* **2009**, *19*, 455; c) I. A. Schepetkin, M. T. Quinn, *Int. Immunopharmacol.* **2006**, *6*, 317.
[20] C. C. Reed, A. Waterhouse, S. Kirby, P. Kay, R. T. Owens, D. J. McQuillan, R. V. Iozzo, *Oncogene* **2005**, *24*, 1104.
[21] Y. Yoon, E. Lee, J. Park, M. Kim, J. Lee, T. Kim, M. Na, J. Kim, *Biotechnol. Bioprocess Eng.* **2011**, *16*, 1099.
[22] G. Tincer, S. Yerlikaya, F. C. Yagci, T. Kahraman, O. M. Atanur, O. Erbatur, I. Gursel, *Biomaterials* **2011**, *32*, 4275.
[23] L. J. Guilbert, B. Winkler-Lowen, A. Smith, D. R. Branch, M. Garcia-Lloret, *J. Leukocyte Biol.* **1993**, *54*, 65.
[24] T. G. Iversen, T. Skotland, K. Sandvig, *Nano Today* **2011**, *6*, 176.
[25] a) N. Tang, G. Du, N. Wang, C. Liu, H. Hang, W. Liang, *J. Natl. Cancer Inst.* **2007**, *99*, 1004; b) S. Meschini, M. Marra, A. Calcabrini, E. Monti, M. Gariboldi, E. Dolfini, G. Arancia, *Toxicol. In Vitro* **2002**, *16*, 389.
[26] S. T. Stern, P. P. Adiseshaiah, R. M. Crist, *Part. Fibre Toxicol.* **2012**, *9*, 20.
[27] S. Rattanakiat, M. Nishikawa, H. Funabashi, D. Luo, Y. Takakura, *Biomaterials* **2009**, *30*, 5701.
[28] G. T. Hermanson, *Bioconjugate Techniques*, Elsevier, Amsterdam, Netherlands **2008**.
[29] a) Y. Wang, L. Chen, Y. Ding, W. Yan, *Int. J. Pharm.* **2012**, *422*, 409; b) Y. Wang, J. Hao, Y. Li, Z. Zhang, X. Sha, L. Han, X. Fang, *Biomaterials* **2012**, *33*, 4741.
[30] a) H. C. Arora, M. P. Jensen, Y. Yuan, A. Wu, S. Vogt, T. Paunesku, G. E. Woloschak, *Cancer Res.* **2012**, *72*, 769; b) X. B. Xiong, Z. Ma, R. Lai, A. Lavasanifar, *Biomaterials* **2010**, *31*, 757.